Heliyon 10 (2024) e34211

Contents lists available at ScienceDirect

Heliyon

journal homepage: www.cell.com/heliyon

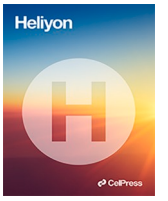

Research article

Albumin incorporation into recognising layer of HER2-specific magnetic nanoparticles as a tool for optimal targeting of the acidic tumor microenvironment

Olga A. Kolesnikova [a], Elena N. Komedchikova [a,e], Svetlana D. Zvereva [a,e], Anastasiia S. Obozina [a], Olha V. Dorozh [a], Iurii Afanasev [a,e], Petr I. Nikitin [b], Elizaveta N. Mochalova [a,c,e], Maxim P. Nikitin [a,c,d], Victoria O. Shipunova [a,c,d,*]

[a] *Moscow Center for Advanced Studies, Kulakova str. 20, 123592, Moscow, Russia*
[b] *Prokhorov General Physics Institute, Russian Academy of Sciences, 38 Vavilov Street, 119991, Moscow, Russia*
[c] *Department of Nanobiomedicine, Sirius University of Science and Technology, 1 Olympic Ave., 354340, Sochi, Russia*
[d] *Shemyakin-Ovchinnikov Institute of Bioorganic Chemistry, Russian Academy of Sciences, 16/10 Miklukho-Maklaya St., 117997, Moscow, Russia*
[e] *Moscow Institute of Physics and Technology, 9 Institutskiy Per., 141701, Dolgoprudny, Russia*

ARTICLE INFO

Keywords:
Magnetic nanoparticles
Affibody
HER2
Theranostics
Targeted delivery
BSA
MPQ

ABSTRACT

Cancer is unquestionably a global healthcare challenge, spurring the exploration of novel treatment approaches. In recent years, nanomaterials have garnered significant interest with the greatest hopes for targeted nanoformulations due to their cell-specific delivery, improved therapeutic efficacy, and reduced systemic toxicity for the organism. The problem of successful clinical translation of nanoparticles may be related to the fact that most in vitro tests are performed at pH values of normal cells and tissues, ranging from 7.2 to 7.4. The extracellular pH values of tumors are characterized by a shift to a more acidic region in the range of 5.6–7.0 and represent a crucial target for enhancing nanoparticle delivery to cancer cells. Here we show the method of non-active protein incorporation into the surface of HER2-targeted nanoparticles to achieve optimal cellular uptake within the pH range of the tumor microenvironment. The method efficacy was confirmed in vitro and in vivo showing the maximum binding of nanoparticles to cells at a pH value 6.4. Namely, fluorescent magnetic nanoparticles, modified with HER2-recognising affibody $Z_{HER2:342}$, with proven specificity in terms of HER2 recognition (with 62-fold higher cellular uptake compared to control nanoparticles) were designed for targeting cancer cells at slightly acidic pH values. The stabilizing protein, namely, bovine serum albumin, one of the major blood components with widespread availability and biocompatibility, was used for the decoration of the nanoparticle surface to alter the pH response of the targeting magnetic

Abbreviations: ADAPT, Albumin-binding domains derived affinity protein; BSA, bovine serum albumin; CMD, carboxymethyl dextran; Cy5, sulfo-Cyanine5 NHS-ester; DMSO, dimethylsulfoxid; DMEM, Dulbecco's modified Eagle's medium; DARPin, Designed Ankyrin Repeat Protein; EDC, 1-ethyl-3-(3-dimethyl aminopropyl) carbodiimide; EGFR, epidermal growth factor receptor family; FITC, fluorescein isothiocyanate; FBS, fetal bovine serum; HER2, human epidermal growth factor receptor 2; IACUC, Institutional Animal Care and Use Committee; ID, injected dose; IPTG, isopropyl ß-D-1-thiogalactopyranoside; MNP, magnetic nanoparticles; MPQ, magnetic particle quantification; MFI, median fluorescence intensities; MRI, magnetic resonance imaging; MES, morpholino ethanesulfonic acid; sulfo-NHS, N-hydroxysulfosuccinimide; NTA, nanoparticle tracking analysis; PEG, polyethylene glycol; PBS, phosphate-buffered saline; RBC, red blood cells; SDS, sodium dodecyl sulfate; SEM, scanning electron microscopy; TEM, transmission electron microscopy; TEMED, tetramethylethylenediamine.

* Corresponding author. Moscow Center for Advanced Studies, Kulakova str. 20, 123592, Moscow, Russia.
E-mail address: shipunova.vo@gmail.com (V.O. Shipunova).

https://doi.org/10.1016/j.heliyon.2024.e34211
Received 25 June 2024; Accepted 5 July 2024
Available online 6 July 2024

conjugates. The optimally designed nanoparticles showed a bell-shaped dependency of interaction with cancer cells in the pH range of 5.6–8.0 with maximum cellular uptake at pH value 6.4 close to that of the tumor microenvironment. In vivo experiments revealed that after i.v. administration, BSA-decorated nanoparticles exhibited 2 times higher accumulation in tumors compared to magnetic nanoparticles modified with affibody only. Thus, we demonstrated a valid method for enhancing the specificity of targeted nanoparticle delivery to cancer cells without changing the functional components of nanoparticles.

1. Introduction

Cancer is a serious global health issue and the second leading cause of death worldwide with commonly diagnosed cancer of the breast, lung, and prostate [1,2]. Conventional cancer therapies such as surgery, chemotherapy, immuno- and radiation therapy are widely used but possess serious side effects, including low efficiency in metastatic tumor treatment, resistance of cancer cells to therapeutic agents, and damage of normal cells outside the treatment site.

Breast cancer among women accounts for 1 in 4 cancer cases and 1 in 6 cancer deaths across the vast majority of countries [3]. This cancer is divided into several types depending on the expression level of the estrogen receptor, progesterone receptor and the human epidermal growth factor receptor 2 (HER2). HER2 belongs to the epidermal growth factor receptor family (EGFR) and is frequently expressed in epithelial, mesenchymal, and neuronal tissues. The overexpression of receptor HER2 in human breast carcinomas is associated with metastasis of cancer, recurrence, and high mortality among patients. In the treatment of HER2-positive breast cancer chemotherapy approaches and targeted molecules for receptor HER2 (antibodies, tyrosine kinase inhibitors) are used to achieve the best outcomes, but mortality from this type of cancer still remains high.

The above-described challenges in cancer treatment can be overcome by the development of different oncotheranostic agents, which present nanoparticle-based structures with diagnostic and therapeutic modalities for selective binding to molecular cancer targets. Nanotheranostic agents can be constructed from a wide range of materials, including protein, polymer, gold, silica, and other organic and inorganic materials [4]. Among the wide variety of nanoparticles, magnetic nanoparticles have proven to be one of the most effective oncotheranostic nanoagents due to their biocompatibility, biodegradability, small size, delivery and visualization of nanoparticle formulations using external magnetic fields [5,6].

Targeted delivery of nanoagents to the receptor HER2 is traditionally performed by clinically approved monoclonal antibodies, namely, trastuzumab and pertuzumab [7,8]. However, the use of full-size IgG as targeting tools for nanoparticle delivery to cancer cells often leads to a broad range of undesirable side effects, especially in vivo, such as the interaction of antibodies with components of the immune system, treatment-emergent resistance of cells to antibodies and cardiac toxicity [9].

In recent decades, artificial scaffold proteins have emerged as much more effective targeting tools compared to full-size IgG. Namely, 8 kDa affibody molecules, a group of engineered affinity proteins, possess unique properties for biomedical applications, such as resistance to proteolysis, tolerance to extreme pH values and temperatures, N- and C-terms available for genetic engineering and others [10–12]. The efficacy of anti-HER2 affibody molecules is confirmed by the fact that the $Z_{HER2:342}$ (ABY-002) molecule is clinically approved for computed tomography imaging for patients with breast cancer. Moreover, based on ABY-002, the next generation of affibody molecules was developed, in particular, ABY-025 and bivalent affibody ABY-027 [13,14].

Since magnetic nanoparticles are clinically approved for diagnostics and therapy (*e.g.*, Ferumoxytol for the treatment of anemia in patients with renal failure, NanoTherm for the treatment of brain glioblastoma) [15], the combination of magnetic nanoparticles with affibody $Z_{HER2:342}$ represents the fastest clinical translation platform for cancer theranostics in consequence of application for (i) targeting, (ii) imaging and (iii) nanoparticle-mediated hyperthermia.

The development of a nanoagent for diagnostics or therapy typically includes three main steps – i) synthesis and modification, ii) in vitro tests, and iii) in vivo tests. Each step goes through a series of optimizations, and it is important to note that during the second step in vitro, nanoparticles are commonly tested at standard extracellular pH values to evaluate their behavior and interactions with biological systems. Indeed, the extracellular pH in healthy tissues typically ranges from 7.2 to 7.4, which represents a neutral or slightly alkaline environment. However, nanoagents may exhibit reduced specificity of binding with cancer cells in the acidic pH values of the tumors. Tumor cells are characterized by normal intracellular pH, but produced increased amount of ions lead to a shift in extracellular pH in the acidic region. Extracellular pH distribution in human tumors is maintained in the range of 6.4–7.0, although highly acidic tumors with a pH of 5.6 are also reported [16]. Various strategies have been employed to target the slightly acidic pH of tumors, such as pH-sensitive polymers [17,18], pH-triggered ionized materials, and pH-triggered drug release mechanisms [19–21], however, the problem of strictly selective nanomaterials delivery remains unresolved.

Since the receptor HER2 is expressed to a certain degree in normal tissues, the extracellular pH level of the tumor microenvironment can be employed as the second combinative target along with HER2 overexpression for enhancing the specificity of nanoparticles binding to HER2-positive cancer cells. Here we introduce the strategy for modifying the surface of nanoparticles with the specific targeting molecule affibody $Z_{HER2:342}$ and the non-active stabilizing protein for the most effective delivery to cancer cells only at slightly acidic pH values. A selected combination of two oppositely charged molecules in an optimal ratio on the MNP surface allows to achieve favorable targeting according to a mechanism that will be described further. We performed screening of HER2-targeted nanoparticles under different conjugation conditions, including different ratios of HER2-targeting and stabilizing proteins, to get nanoagents for selective targeting of HER2-positive cancer cells at pH values of tumor microenvironment. The synthesized magnetic

nanoparticles were functionally tested in vitro and in vivo and demonstrated 2-fold higher accumulation in tumor allografts in vivo compared to control conjugates. Therefore, the obtained magnetic nanoparticles possess significant potential in the development approaches for tumor targeting, bioimaging, and treatment.

2. Materials and methods

2.1. Materials

Sigma, Darmstadt, Germany: sodium phosphate dibasic, sodium phosphate monobasic, N-(3-Dimethylaminopropyl)-N-ethyl-carbodiimide hydrochloride, dimethyl sulfoxide, carboxymethyl dextran, iron (III) chloride hexahydrate, iron (II) sulfate heptahydrate, sodium dodecyl sulfate, boric acid. Paneco, Moscow, Russia: Versene solution, L-glutamine, penicillin-streptomycin, gentamicin, and bovine serum albumin. HyClone, Logan, UT, USA: DMEM medium and fetal bovine serum. Dia-M, Moscow, Russia: ammonium hydroxide, potassium dihydrogen phosphate. Lumiprobe, Moscow, Russia: sulfo-Cyanine5 NHS-ester. Thermo Fisher Scientific, Waltham, MA, USA: N-hydroxysulfosuccinimide and Fluorescein isothiocyanate. AppliChem, Darmstadt, Germany: sodium chloride. Chimmed, Moscow, Russia: n-hexane, n-butanol, ethanol. Chemical line, Saint Petersburg, Russia: sodium chloride, potassium chloride. AppliChem, Darmstadt, Germany: 2-(N-morpholino)ethanesulfonic acid.

2.2. Synthesis of MNP

Magnetic nanoparticles (MNP) were synthesized by microemulsion method using organic solvents as an oil phase. Firstly, 2 g of sodium dodecyl sulfate (SDS) was dissolved in a mixture consisting of 20 mL of n-hexane and 12 mL of n-butanol. The obtained solution was homogenized by sonication and heated at 40 °C in a glass flask for 20 min under magnetic stirring. Next, 0.5 M $FeSO_4$ in 0.6 mL of Milli-Q water was added to the organic emulsion and 2 min later 0.5 M $FeCl_3$ in 1 mL of Milli-Q water was added to the solution to receive an orange-colored solution. The temperature of the mixture was maintained at 40 °C for 20 min under magnetic stirring. After this step, the solution was heated to 70 °C and 2 mL of NH_4OH was added dropwise while magnetic stirring to obtain the black-colored solution. The obtained mixture was mixed under magnetic stirring for 1 h with a maintained temperature of 70 °C. After this stage, the solution was cooled to room temperature, the organic solution was removed from the flask and EtOH was added. The obtained magnetic NPs were magnetically separated and washed 3 times from the organic solvent with EtOH and then washed 3 times from EtOH with Milli-Q water.

2.3. Electron microscopy

MNP were characterized by scanning electron microscopy (SEM) and transmission electron microscopy (TEM). SEM images were obtained by using a MAIA3 electron microscope (Tescan, Czech Republic) at an accelerating voltage of 5 kV. The samples were deposited onto a silicon wafer on carbon film and air-dried at room temperature. TEM images were performed by using a JEM-2100plus transmission electron microscope (JEOL, Japan) with an accelerating voltage of 200 kV. The samples were applied at formvar/carbon film on a gold grid and air-dried at room temperature. Particle size distribution was obtained from the analysis of several SEM microphotographs using ImageJ software and counting a minimum of 100 nanoparticles.

2.4. Polymer coating of the surface of MNP

Carboxymethyl dextran (CMD) was covalently bound to the surface of previously washed magnetic nanoparticles. 100 μL of MNP and 300 μL of CMD solution at 300 g/L in Milli-Q water were used for the reaction. The mixture was stirred using ultrasound and then incubated for 5 min at 90 °C in a water bath. Next, the nanoparticles were cooled for 5 min at 4 °C. These manipulations were repeated 3 times, after which the nanoparticles were left overnight and then washed from the unbound polymer three times with Milli-Q water.

2.5. DLS measurements

The hydrodynamic diameter of uncoated MNP and CMD-coated MNP were measured by dynamic light scattering technique using Malvern Zetasizer Nano ZS (Malvern Instruments, UK). To perform this analysis, several samples were prepared: MNP resuspended in Milli-Q water, MNP resuspended in PBS, CMD-coated MNP resuspended in Milli-Q water and CMD-coated MNP resuspended in PBS.

2.6. Nanoparticle tracking analysis

The nanoparticle tracking analysis (NTA) technique is capable of measuring the concentration of nanoparticles, scattering intensity, and hydrodynamic diameter simultaneously. NTA uses the relative scattering intensities as a function of the refractive index and allows the distinction of nanoparticles with comparable diameters ranging from 3 nm to 1000 nm. CMD-coated MNP were prepared in 10 % glucose solution at concentrations of 1 g/L and 0.001 g/L. Particles in the sample were analyzed with an NTA device (Abisense, Russia), which visualizes individual nanoparticles by detection of scattered light. The trajectories of nanoparticles in the field of view were recorded and analyzed with the Stokes-Einstein equation, which measures the mean squared displacement $\underline{(x,y)^2}$ of

the NP in two dimensions: $\underline{(x,y)^2} = \frac{3k_BT}{3R_H\pi\eta}$.

2.7. Expression and purification of affibody $Z_{HER2:342}$

E. coli strain BL21 (DE3), transformed with the pET39-Z342 gene, was grown in 500 mL 2 YT medium containing 100 μg/mL kanamycin for 24 h at 37 °C. Protein expression was induced using 1 mM isopropyl ß-D-1-thiogalactopyranoside and overnight shaking at 37 °C. The cells were harvested by centrifugation at 3400*g* at 4 °C for 30 min and resuspended in lysis buffer (20 mM Na-Pi, 300 mM NaCl, pH 7.5, 50 μg/mL lysozyme). The suspension was incubated on ice for 30 min. Cells were sonicated on ice with the Bandelin Sonopuls HD2200 (Bandelin, Germany). Cell debris was centrifuged at 10 000 g at 4 °C for 30 min. The protein was purified from the lysate using Ni-AZUR resin (Abisense, Russia) using affinity chromatography under native conditions. Lysate was incubated with 2 mL of Azur Agarose for 1 h using gentle agitation to keep the resin suspended. Next, the suspension was placed into a purification column and settled by low-speed centrifugation (500 g). The resin was washed 3 times with 5 column volumes of wash buffer (20 mM Na-Pi, 300 mM NaCl, 10 mM Imidazole). The bound protein was eluted with 2 mL of elution buffer (20 mM Na-Pi, 300 mM NaCl) with various concentrations of imidazole (50, 100, 150, 200, 250, and 500 mM).

The elution fractions were analyzed by SDS-PAGE (15 %) using the Tris-glycine electrophoresis system consisting of a separating gel (14.7 % acrylamide/0.3 % bisacrylamide, 0.1 % ammonium persulfate, 0.08 % TEMED, 0.1 % SDS, 375 mM Tris·Cl, pH 8.8), a stacking gel (3.9 % acrylamide/0.1 % bisacrylamide, 0.1 % ammonium persulfate, 0.001 % TEMED, 0.1 % SDS, 0.13 M Tris·Cl, pH 6.8), an electrophoresis buffer (0.025 M Tris base, pH 8.9, 250 mM Glycine, 0.1 % SDS), and a sample buffer (10 % glycerol, 1 % SDS, 0.02 % Bromphenol blue, 0.1 M b-MeEtOH, 0.05 M Tris·Cl, pH 6.8). The fractions on the gel were visualized with a Coomassie blue staining.

All elution fractions containing affibody were combined and concentrated using Pierce Protein Concentrator PES, 3 K MWCO. Protein concentration was determined by BCA protein assay. The protein content was also confirmed with the Nanodrop UV–Vis spectrophotometer (Thermo Fisher Scientific, USA).

2.8. Fluorescent labeling of affibody $Z_{HER2:342}$ with FITC

For the labeling reaction, 100 μg of affibody $Z_{HER2:342}$ and 10 μL of fluorescein isothiocyanate **(**FITC) in dimethylsulfoxide (DMSO) at a concentration of 7 g/L were mixed and incubated overnight at room temperature. The excess of unreacted reagents was removed using Zeba Spin Desalting Columns, 7 MWCO.

2.9. Covalent modification of the surface of MNP with proteins

Previously obtained CMD-coated MNP were modified with 2 proteins: HER2-recognising affibody $Z_{HER2:342}$ and bovine serum albumin (BSA) as a control. Proteins were covalently coupled to the surface of MNP using the standard bioconjugation method with 1-ethyl-3-(3-dimethyl aminopropyl) carbodiimide (EDC) and N-hydroxysulfosuccinimide (sulfo-NHS) as cross-linking agents. Firstly, EDC/sulfo-NHS solution in 0.1 M morpholino ethanesulfonic acid (MES) with pH 5.0 was added to MNP for activation of carboxyl groups on the surface of CMD-coated MNP for 15 min. Then, the excess of crosslinkers was removed by magnetic separation. In the next stage, proteins were prepared in borate buffer, containing 0.4 M H_3BO_3 and 70 mM $Na_2B_4O_7{\cdot}10H_2O$ with pH 8.0.70 μg of proteins in buffer were added to MNP and incubated at 4 °C overnight, then unreached proteins were removed by magnetic separation.

For the experiment with different amounts of affibody $Z_{HER2:342}$ conjugated to the surface of MNP, several concentrations of protein were used during the chemical reaction: 20 μg of affibody $Z_{HER2:342}$ to 1 mg of MNP (MNP-AF1), 47 μg of affibody $Z_{HER2:342}$ to 1 mg of MNP (MNP-AF2), 93 μg of affibody $Z_{HER2:342}$ to 1 mg of MNP (MNP-AF3), 160 μg of affibody $Z_{HER2:342}$ to 1 mg of MNP (MNP-AF4), 334 μg of affibody $Z_{HER2:342}$ to 1 mg of MNP (MNP-AF5).

For the experiment with the addition of bovine serum albumin in the bioconjugation process, several concentrations of proteins were used: 93 μg of affibody $Z_{HER2:342}$ and 930 μg of bovine serum albumin to 1 mg of MNP (MNP-AF-BSA1), 93 μg of affibody $Z_{HER2:342}$ and 279 μg of bovine serum albumin to 1 mg of MNP (MNP-AF-BSA2), 93 μg of affibody $Z_{HER2:342}$ and 93 μg of bovine serum albumin to 1 mg of MNP (MNP-AF-BSA3), 930 μg of bovine serum albumin to 1 mg of MNP (MNP-BSA), 93 μg of affibody $Z_{HER2:342}$ to 1 mg of MNP (MNP-AF).

In the next stage, MNP modified with proteins were fluorescently labeled by using sulfo-cyanine5 NHS ester (Cy5). Conjugates were prepared by mixing 1 mg of MNP with 10 μg of Cy5 in Milli-Q water, the mixture was incubated for 12 h at 4 °C. Then the excess of unreached dye was removed by magnetic separation, and nanoparticles were washed eight times with phosphate-buffered saline (PBS), containing 137 mM NaCl, 2.7 mM KCl, 10 mM Na_2HPO_4, 1.8 mM KH_2PO_4, adjusting pH value to 7.4 using NaOH.

2.10. Calculating the number of affibody molecules on the surface of a single MNP

MNP-AF1 – MNP-AF5 conjugates after incubation with the protein in the borate buffer were magnetically separated from unbound protein. The protein from the supernatant was analyzed using the BCA Protein Assay Kit (Abisense, Russia). Reagent 1 was mixed with Reagent 2 at a ratio of 50:2 and dropped into a 96-well assay plate. Control samples of affibody with a known concentration in the range of 0.1–2 g/L were prepared in PBS. Control or protein solution under investigation was added to each well of the plate in a ratio of 1:10 to the volume of the well. The obtained solution was mixed for 20 min at room temperature. After incubation, the absorbance at 562 nm was measured. The quantity of protein per 1 mg of MNP was calculated by a calibration curve. The number of conjugated

affibody molecules per single nanoparticle was evaluated by recalculating the amount of conjugated protein to the number of nanoparticles per mL. Based on the above measurements, the following data were obtained: 24 affibody molecules per single MNP (MNP-AF1), 57 affibody molecules per single MNP (MNP-AF2), 114 affibody molecules per single MNP (MNP-AF3), 122 affibody molecules per single MNP (MNP-AF4), 238 affibody molecules per single MNP (MNP-AF5).

2.11. ζ-potential measurements

ζ-potential was measured by electrophoretic light scattering technique using Malvern Zetasizer Nano ZS (Malvern Instruments, UK). To perform this analysis, five magnetic conjugates were resuspended in PBS: MNP, MNP-AF-BSA1, MNP-AF-BSA2, MNP-AF-BSA3, MNP-BSA, and MNP-AF.

2.12. Buffer system for in vitro tests

Firstly, stock solutions of 0.5 M NaH_2PO_4, 0.5 M Na_2HPO_4, and 5 M NaCl were prepared. Buffer 1 with a pH value of 5.5 and buffer 2 with a pH value of 8.0 were obtained by mixing the stock solutions with Milli-Q water and fetal bovine serum (FBS). The final composition of buffer 1 included 50 mM NaH_2PO_4, 100 mM NaCl, and 10 % FBS, while buffer 2 contained 50 mM Na_2HPO_4, 100 mM NaCl, and 10 % FBS. Eight buffers within a pH value in a range of 5.6–8.0 were prepared by combining varying proportions of buffer 1 and buffer 2.

2.13. Cy5 fluorescence measurement

To measure the Cy5 fluorescence intensity at different pH values, the solution of Cy5 in saline buffers at a concentration of 5 mg/L was prepared. 100 μL of the obtained mixture was added to a 96-well plate and fluorescent imaging was performed with a LumoTrace FLUO bioimaging system (Abisense, Russia) with 630 nm excitation wavelength and 650LP nm emission filter, and exposure of 500 ms.

2.14. Cell culture

EMT6/P cells (a mouse mammary cell line, ECACC collection) and EMT-HER2 cells (EMT6/P cells with transduced receptor HER2 obtained in our previous work [22]) were cultured in Dulbecco's modified Eagle's medium (DMEM) supplemented with 10 % heat-inactivated fetal bovine serum, 2 mM L-glutamine, sodium pyruvate, and antibiotics (penicillin/streptomycin, gentamicin). Cells were incubated at 37 °C in a humidified atmosphere with 5 % CO_2.

2.15. Cell viability in buffer systems

For this analysis EMT-HER2 cell line was used: 150×10^3 cells were incubated in saline buffers with pH values in the range of 5.6–8.0 for 30 min. Then cells were washed 3 times from solutions with PBS with 1 % BSA and seeded on a 96-well plate at concentration of 2×10^3 cells per well in 100 μL of DMEM supplemented with 10 % heat-inactivated fetal bovine serum. The cells were cultured for 3 days, then cellular viability was analyzed by using of resazurin-test. The medium solution was removed from wells, resazurin solution (13 mg/L in PBS) was added to each well and the cells were incubated for 2 h at 37 °C in a humidified atmosphere with 5 % CO_2. The fluorescence signal from each well was measured by CLARIOstar microplate reader (BMG Labtech, Germany) at wavelengths of λex = 570 nm, λem = 600 nm. Data are presented as percent from the cells incubated in solution with the standard pH value of 7.4.

2.16. Flow cytometry

For the analysis of FITC-labeled affibody $Z_{HER2:342}$ binding efficiency, 1 μg of fluorescently-labeled protein was mixed with 150×10^3 cells (EMT6/P and EMT-HER2 cells) in 150 μL of PBS with 1 % BSA. Cells were incubated for 30 min and then washed 3 times from unbound protein by centrifugation. Flow cytometry analysis was performed using the Novocyte 2000R flow cytometer (ACEA Biosciences, USA) in the BL1 channel (excitation laser 488 nm, emission filter 530/30 nm).

For the analysis of magnetic conjugates' interaction with EMT-HER2 cancer cells at different pH values, 102 μg for minimal concentration (1), 220 μg for middle concentration (2), and 365 μg for maximal concentration (3) of magnetic conjugates were mixed with 150×10^3 cells in 100 μL of buffers with pH values in the range of 5.6–8.0. Cells were incubated for 30 min and washed 3 times from unbound nanoparticles with buffers of corresponding pH values. After washing, the cells were transferred to a PBS (pH 7.4) and analyzed with the Novocyte 2000R flow cytometer in the following channel: λex = 640 nm, λem = 675/30 nm.

The interaction of MNP with different amounts of conjugated affibody $Z_{HER2:342}$ (MNP-AF1 – MNP-AF5) with EMT-HER2 cells was studied as follows: 102 μg of MNP was mixed with 150×10^3 cells in 100 μL of buffers with pH values in the range of 5.6–8.0. Washing from unbound MNP and analysis were performed with the Novocyte 2000R flow cytometer in the following channel: λex = 640 nm, λem = 675/30 nm.

To determine nanoparticles with conjugated affibody $Z_{HER2:342}$ and BSA (MNP-AF-BSA1, MNP-AF-BSA2, MNP-AF-BSA3, MNP-AF, MNP-BSA) EMT-HER2 cell-binding efficiency, all steps as for MNP-AF1 – MNP-AF5 were repeated.

2.17. Fluorescent microscopy

Visualization of the interaction of affibody $Z_{HER2:342}$-FITC with cells was performed as follows: EMT-HER2 cells and EMT6/P cells as control were seeded on 96-well plate at 10×10^3 cells per well in 100 μL of DMEM supplemented with 10 % FBS and cultured overnight. In the next stage, cells were incubated with 1 μg/mL of affibody $Z_{HER2:342}$-FITC for 15 min in PBS at room temperature and washed from unbound proteins. Confocal laser scanning microscopy imaging was carried out using the FV3000 laser-scanning confocal microscope (Olympus Optical Co. Ltd., Tokyo, Japan) with a 488 nm laser and emission detector of 500–600 nm.

The confocal microscopy images of MNP-BSA and MNP-AF-BSA binding with EMT-HER2 cells were obtained as follows: EMT-HER2 cells were seeded on a 96-well plate at 10×10^3 cells per well in 100 μL of DMEM supplemented with 10 % FBS and cultured overnight. Then, cells were incubated with 0.3 mg/mL of MNP for 30 min at 4 °C and washed from unbound nanoparticles thrice with PBS with 1 % BSA. Cells were analyzed by fluorescence microscopy with epifluorescent Zeiss microscope at the following conditions: excitation filter −595–645 nm, emission filter −670–725 nm.

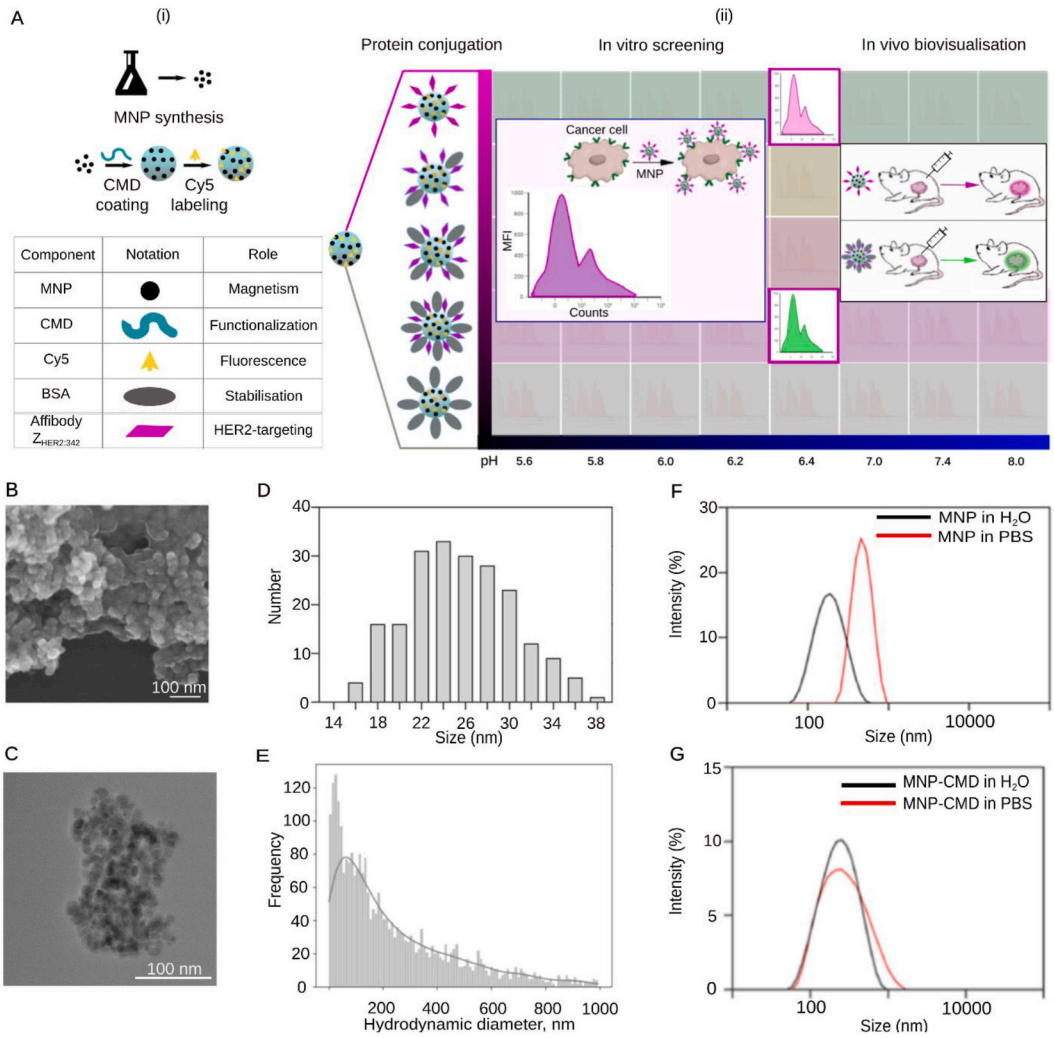

Fig. 1. Magnetic nanoparticle synthesis and characterization. (A) Scheme of experiment: (i) fluorescent carboxymethyl-dextran-coated MNP functionalization with affibody $Z_{HER2:342}$ and decoration with bovine serum albumin; (ii) screening the optimal HER2-specific magnetic nanoparticle for targeting cancer cells in pH value of the tumor microenvironment and biodistribution study of the selected conjugate in vivo. (B) Scanning electron microscopy micrograph of MNP, scale bar 100 nm. (C) Transmission electron microscopy images of nanoparticles, scale bar 100 nm. (D) Histogram of MNP size distribution obtained by SEM image processing. (E) Hydrodynamic particle size distribution by frequencies obtained for MNP-CMD in H_2O by nanoparticle tracking analysis. (F) Hydrodynamic particle size distribution by intensities obtained for MNP in H_2O and PBS. (G) Hydrodynamic particle size distribution by intensities obtained for MNP-CMD in H_2O and PBS.

2.18. Tumor-bearing mice

Male BALB/c mice of 20–25 g weight were purchased from the Puschino Animal Facility (Shemyakin-Ovchinnikov Institute of Bioorganic Chemistry Russian Academy of Sciences, Pushchino branch of the Institute, Pushchino, Russia) and maintained at the Vivarium of the Shemyakin-Ovchinnikov Institute of Bioorganic Chemistry Russian Academy of Sciences (Moscow, Russia). All experimental procedures were approved by the Institutional Animal Care and Use Committee (IACUC) of the Shemyakin-Ovchinnikov Institute of Bioorganic Chemistry Russian Academy of Sciences (Moscow, Russia), protocol # 375/2023 (20 September 2023–September 19, 2026). Mice were subcutaneously injected with 3×10^6 EMT-HER2 cells in 100 μL of serum-free culture media into the right flank to create tumor allografts. Biodistribution studies were started 14 days after inoculation.

2.19. Biodistribution of MNP in mice

Tumor-bearing mice were i.v. injected with 1 mg of MNP through the retroorbital sinus injection. Then, 16 h after injection mice were anesthetized with a mixture of Zoletil (Virbac, France) and Rometar (Bioveta, Czech Republic) and placed into a chamber of LumoTrace FLUO bioimaging tomograph (Abisense, Russia). Fluorescent images of mice were received with excitation wavelength of 630 nm, 650LP nm emission filter, and exposure of 2000 ms.

2.20. MPQ-measurements

After studying MNP biodistribution in vivo, mice were euthanized and organs were extracted. Magnetic signals in organs were measured using our original MPQ device [23].

2.21. Magnetic resonance imaging (MRI)

1 mg of MNP-AF or MNP-AF-BSA in 100 μL of PBS were intravenously injected into BALB/c mice. Then mice were euthanized and imaged with an ICON 1T MRI system (Bruker, USA) using a mouse whole-body-volume radiofrequency coil. Non-injected BALB/c mice were used as control. We applied FLASH sequence with the following parameters: repetition time – 1000 ms, echo time – 5 ms, flip angle – 60°, field-of-view – 8/5 cm, 17 slices per scan, slice thickness – 1 mm.

3. Results

3.1. Design of experiment

The design of the research is schematically presented in Fig. 1A, which includes two parts:

(i) Synthesis, characterization, and modification of magnetic nanoparticles. Nanoparticles were synthesized by the microemulsion method, stabilized with carboxymethyl-dextran polymer, and characterized by electron microscopy. Then, the obtained nanoparticles were modified with two proteins: HER2-recognising molecule, namely, affibody $Z_{HER2:342}$, and bovine serum albumin. Magnetic conjugates were labeled with the fluorescent dye Cy5, which is characterized by fluorescence emission in the transparency window of biological tissues, for visualization of cell*nanoparticle complexes.

(ii) Screening the optimal magnetic conjugate for interaction with cancer cells at slightly acidic pH in vitro and in vivo. First, five types of magnetic conjugates with affibody and/or BSA were studied for the specificity of interaction with HER2-positive cancer cells at pH values in the range of 5.6–8.0. Then, magnetic conjugate with maximal cellular uptake at the pH value of the tumor microenvironment and control magnetic nanoparticles were injected into HER2-positive tumor-bearing mice to visualize the tumor location and analyze the distribution of nanoparticles in vivo.

3.2. Synthesis and characterization of magnetic nanoparticles

MNP were synthesized by the water-in-oil microemulsion method as described by us previously [8]. Briefly, a water phase containing Fe^{3+}/Fe^{2+} ions was added to the oil phase with surfactants, the obtained solution was heated to 70 °C, and NH_4OH aqueous solution was added for precipitation of MNP.

The synthesized MNP were characterized by SEM and TEM. Fig. 1B and C present SEM and TEM images of obtained MNP. The size of the nanoparticles was characterized by processing SEM microphotographs using ImageJ software. Fig. 1D demonstrates the nanoparticle size distribution, the average size of MNP was 25.2 ± 5.4 nm.

Colloidal stability of MNP in saline solutions, namely, the ability of nanoparticles to remain dispersed without aggregation or precipitation, is a crucial parameter for *vitro* and in vivo studies that are used as models of physiological conditions. To stabilize nanoparticles in saline solutions, a stable coating of nanoparticle surface with a biocompatible polymer, namely, carboxymethyl-dextran was used. Moreover, CMD polymer that possesses terminal –COOH groups was previously shown to be an effective intermediate coating of nanoparticle surface for further chemical conjugation to different protein molecules through carbodiimide (EDC/NHS) chemistry [24,25]. Fig. 1F and G demonstrate successful coating and stabilization of MNP with CMD. Namely, the hydrodynamic sizes of uncoated MNP and CMD-coated MNP in water showed no significant difference and were 201 ± 81 nm and 266 ± 140 nm,

respectively. CMD-coated MNP demonstrated stability in saline solution with the hydrodynamic size of 329 ± 229 nm, whereas the hydrodynamic size of uncoated MNP was changed significantly compared to aqueous solution and was 686 ± 233 nm.

To carry out the quantitative analysis of CMD-coated MNP, namely, to quantify the concentration of nanoparticles, the NTA was performed using an AstraTrace device (Abisense, Russia, Fig. S1). The number of MNP at concentration 1 g/L was calculated and found to be equal to 7.32×10^{16} MNP/L. The stabilization efficiency of the CMD polymer was also confirmed by NTA, the hydrodynamic size distribution of CMD-coated MNP is presented in Fig. 1E with an average size of 182 ± 15 nm.

3.3. *Affibody $Z_{HER2:342}$ as a targeting molecule for nanoparticle delivery to HER2-positive cancer cells*

Targeted delivery of MNP to HER2-positive cancer cells was ensured by the functionalization of MNP surface with anti-HER2 affibody $Z_{HER2:342}$. Our previous studies demonstrated that affibody $Z_{HER2:342}$ significantly outperforms other HER2-recognising protein agents (scaffold protein DARPin G3 and full-size IgG trastuzumab) for targeted delivery of magnetic and polymer nanoparticles to HER2-positive cancer cells [8,26]. Affibody $Z_{HER2:342}$ was produced in *E. coli* strain BL21 (DE3) and purified through metal chelate affinity chromatography. The result of electrophoretic separation of affibody by SDS-PAGE is shown in Fig. 2A and indicates

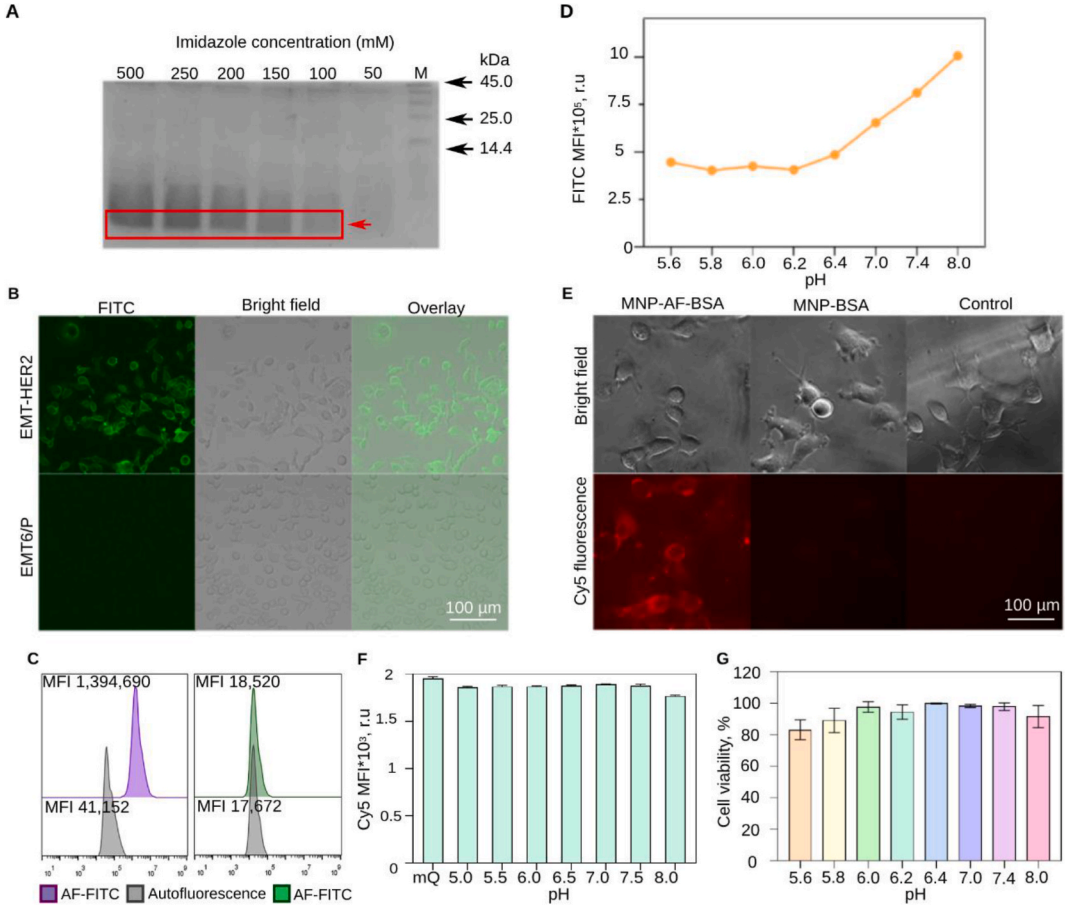

Fig. 2. Affibody $Z_{HER2:342}$ as a HER2-recognising molecule for targeted delivery of nanoparticles to cancer cells. (A) SDS-PAGE of affibody $Z_{HER2:342}$ from eluted fractions. The red frame demonstrates the target protein fractions. (B) Confocal laser scanning microscopy of EMT6/P and EMT-HER2 cells labeled with affibody $Z_{HER2:}$342-FITC. Left panels – confocal images of the cells (λex = 488 nm, λem = 500–600 nm), middle panels – bright-field images, right panels – overlayed images. Scale bar, 100 μm. (C) Flow cytometry histograms of EMT6/P and EMT-HER2 cells labeled with affibody $Z_{HER2:342}$-FITC with median MFI of FITC (λex = 488 nm, λem = 530/30 nm). Grey color – cells' autofluorescence, green and violet – cells labeled with $Z_{HER2:342}$-FITC conjugates. (D) AF-FITC pH-dependent interaction with EMT-HER2 cells measured with flow cytometry quantitative analysis. The dots represent cell populations at several solutions with pH values in the range of 5.6–8.0 in the fluorescent channel corresponding to the FITC fluorescence (λex = 488 nm, λem = 530/30 nm). (E) Visualization of MNP-BSA and MNP-AF interaction with EMT-HER2 cancer cells by fluorescent microscopy. Top panels – bright-field images, bottom panels – fluorescent images of the cells (λex = 595–645 nm, λem = 670–725 nm). Scale bar, 100 μm. (F) Cy5 fluorescence intensity dependence on the pH level of the solution (within the range of 5.0–8.0). The bars represent the Cy5 fluorescence in the fluorescent channel corresponding to the Cy5 fluorescence (λex = 630 nm, λem = 650LP nm). (G) EMT-HER2 cells pH-dependent viability after incubation in saline buffers with pH values in the range of 5.6–8.0. (For interpretation of the references to color in this figure legend, the reader is referred to the Web version of this article.)

that affibody was presented in each elution fraction. According to the intensity of protein bands on the gel, the higher the concentration of imidazole was, the more affibody molecules eluted. The UV–Vis spectrum of the purified affibody molecule had a single peak at 280 nm and confirmed the protein content, which is presented in Fig. S2A.

To evaluate the specificity of purified affibody in terms of HER2 binding in vitro, purified affibody $Z_{HER2:342}$ was labeled with the fluorescent dye fluorescein isothiocyanate (FITC). Two cell lines were used for this test: EMT-HER2 cells with receptor HER2 over-expression and EMT6/P cells without HER2 expression as a control cell line [22]. EMT6/P and EMT-HER2 cells were incubated with affibody $Z_{HER2:342}$-FITC conjugates (AF-FITC) and analyzed by confocal microscopy (Fig. 2B) and flow cytometry (Fig. 2C). The analysis of median fluorescence intensities (MFI) showed that MFI of EMT-HER2 cells labeled with AF-FITC was 75.3 higher than that for EMT6/P cells, thus proving the high specificity of $Z_{HER2:342}$.

Next, the optimal pH values for the interaction between affibody and the HER2 receptor were established. As can be seen from Fig. 2D, the binding capacity of AF-FITC to HER2-positive cancer cells was minimal at slightly acidic pH values, while the maximal interaction was observed at standard pH range of 7.4–8.0.

3.4. Functionalization of MNP with affibody for targeted delivery to HER2-positive cancer cells

Previously synthesized CMD-coated MNP were used for covalent modification with 2 types of proteins: affibody $Z_{HER2:342}$ for

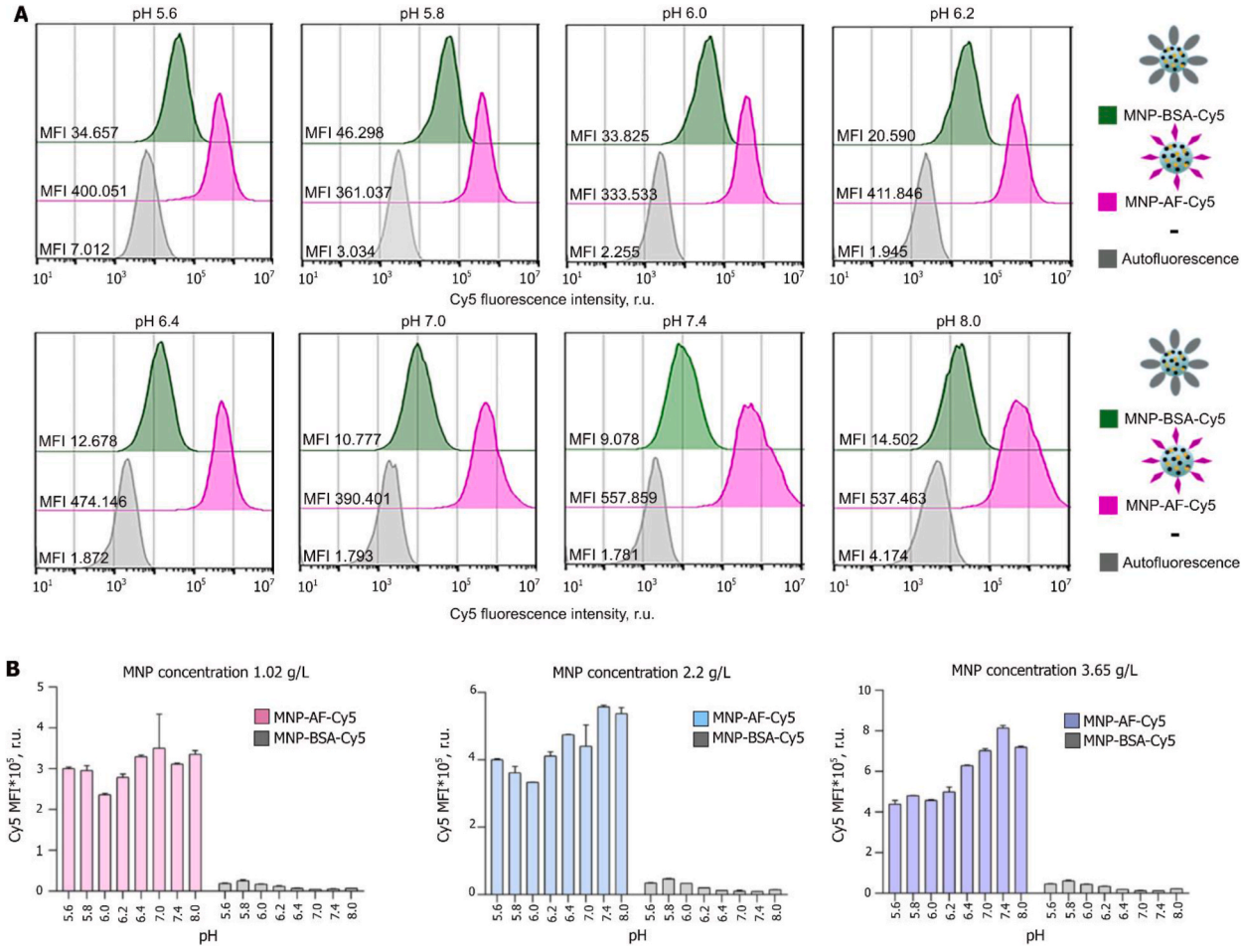

Fig. 3. Screening of affibody-modified MNP for HER2-binding efficiency at various pH values. (A) Flow cytometry histograms of EMT-HER2 cells labeled with MNP-AF-Cy5 and MNP-BSA-Cy5. Histograms represent cell populations in the fluorescent channel corresponding to the Cy5 fluorescence (λex = 640 nm, λem = 675/30 nm). Grey color – cells' autofluorescence, green, pink color – cells with MNP-BSA-Cy5, and MNP-AF-Cy5 conjugates, respectively. (B) Flow cytometry quantitative analysis of MNP binding efficiency to EMT-HER2 at different concentrations of MNP. The bars represent cell populations at several solutions with pH values in the range of 5.6–8.0 in the fluorescent channel corresponding to the Cy5 fluorescence (λex = 640 nm, λem = 675/30 nm). Grey color – cells labeled with MNP-BSA-Cy5 conjugates with different concentrations, pink – cells labeled with MNP-AF-Cy5 conjugates at concentration 1.02 g/L, blue – cells labeled with MNP-AF-Cy5 conjugates at concentration 2.2 g/L, violet – cells labeled with MNP-AF-Cy5 conjugates at concentration 3.65 g/L. (For interpretation of the references to color in this figure legend, the reader is referred to the Web version of this article.)

targeting HER2-positive cancer cells (MNP-AF) and bovine serum albumin to get non-specific nanoparticles for control experiments (MNP-BSA). Conjugation was performed by the standard carbodiimide reaction consisting of 1-ethyl-3-(3-dimethyl aminopropyl) carbodiimide (EDC)-mediated activation of carboxyl groups on the surface of MNP and N-hydroxysulfosuccinimide stabilization of intermediate product through ester formation. In the next stage, nanoparticles were labeled with the fluorescent dye Cy5 with fluorescence emission in the near-infrared wavelength region between 650 and 800 nm. The binding efficiency of targeted conjugate MNP-AF-Cy5 compared to control conjugate MNP-BSA-Cy5 was performed using confocal microscopy and is presented in Fig. 2E. MNP-AF-Cy5 exhibited high cellular uptake by HER2-positive cancer cells compared to control conjugates MNP-BSA-Cy5, as evidenced by the higher fluorescence intensity of cells in the corresponding fluorescence channel (Fig. 2E).

3.5. pH-dependent binding of affibody-modified MNP to HER2-overexpressing cancer cells

First of all, we evaluated the pH dependence of Cy5 fluorescence with the optical tomograph LumoTrace (Abisense, Russia). Fig. 2F shows that the fluorescence intensity of the Cy5 remained relatively constant within the 5.0–8.0 pH range, thus proving the validity of the choice of this dye for fluorescence measurement at different pH values.

The pH-dependent cellular survival in various saline solutions was studied at EMT-HER2 cell line, while cells were shortly incubated in buffers within the pH range of 5.6–8.0. Fig. 2G demonstrates a high level of cell viability except the most acidic pH value, which deviates by almost 2 units from standard cell culture conditions.

In the next step, EMT-HER2 cells were labeled with previously obtained magnetic conjugates in phosphate saline buffers with pH values in the range of 5.6–8.0 and analyzed by flow cytometry. Three concentrations of MNP were chosen for this test, namely, 1.02 g/L (1), 2.2 g/L (2), and 3.65 g/L (3), to investigate the binding specificity of MNP depending on their concentration and pH values. Fig. 3A presents a quantitative analysis for the minimal concentration of MNP (1) and demonstrates the effective and specific

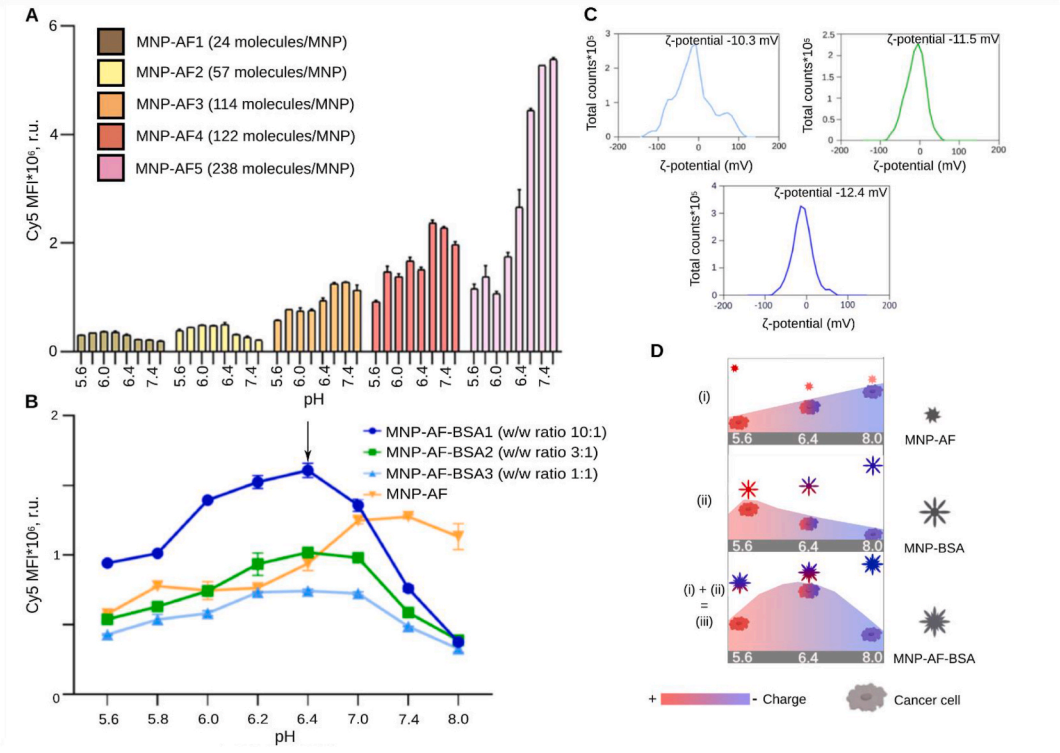

Fig. 4. Screening of affibody-modified MNP for the most effective binding with HER2-overexpressing cancer cells at slightly acidic pH: influence of affibody molecules and presence of non-active stabilizing protein, BSA. (A) Flow cytometry quantitative analysis: EMT-HER2 cells were labeled with MNP conjugated to different numbers of affibody $Z_{HER2:342}$ molecules. The bars represent cell populations at several solutions with pH values in the range of 5.6–8.0 in the fluorescent channel corresponding to the Cy5 fluorescence. Brown, yellow, orange, red, and pink color – cells labeled with MNP-AF1, MNP-AF2, MNP-AF3, MNP-AF4, and MNP-AF5 conjugates, respectively. (B) Flow cytometry quantitative analysis: EMT-HER2 cells were labeled with affibody-functionalized MNP decorated with different stabilizing protein BSA (at different BSA:affibody ratios). The dots represent cell populations at several solutions with pH values in the range of 5.6–8.0 in the fluorescent channel corresponding to the Cy5. Blue, green, and light blue color – cells labeled with MNP-AF-BSA1, MNP-AF-BSA2, and MNP-AF-BSA3 conjugates, respectively. (C) ζ-potential distributions and average ζ-potential of three MNP conjugates: blue color – AF-BSA1 MNP, green – AF-BSA2 MNP, light blue – AF-BSA3 MNP. (D) Proposed mechanism of nanoparticles interaction with EMT-HER2 cells at several solutions with pH values in the range of 5.6–8.0: (i) MNP-AF, (ii) MNP-BSA, (iii) MNP-AF-BSA. A color gradient from red to blue color illustrates changes in the surface charge from negative to positive charge. (For interpretation of the references to color in this figure legend, the reader is referred to the Web version of this article.)

interaction of MNP-AF-Cy5 compared to control conjugates MNP-BSA-Cy5 for all tested pH values. The highest cellular uptake was observed at pH 7.4, where the MFI of EMT-HER2 cells labeled with MNP-AF-Cy5 was 62 higher than that with MNP-BSA-Cy5, respectively. Accordingly, MNP-AF-Cy5 is an optimal conjugate for specific binding with cancer cells at a standard pH 7.4, but not for a slightly acidic pH.

We hypothesized that the binding efficiency of affibody $Z_{HER2:342}$ at acidic pH would be higher due to the positive charge of affibody $Z_{HER2:342}$ with the isoelectric point of 9.1 and the negative charge on the cells at low pH values [27]. However, data presented in Fig. 3B demonstrates that the binding efficiency of MNP-AF-Cy5 increased as the pH value of the buffer was changed to the alkaline region, this trend was observed across all concentrations of the conjugates and correlated with the curve of AF-FITC interaction with the receptor HER2 (Fig. 2D). It can be assumed that affibody*HER2 interaction occurs with a Kd of 22 pM [28–30] and prevails over much weaker electrostatic interaction. The decline in MNP binding efficiency within the slightly acidic pH range can be attributed to a shift in the protein surface charge caused by protonation.

3.6. The number of affibody $Z_{HER2:342}$ molecules on the surface of MNP affects the binding specificity of MNP with cancer cells at acidic pH

The number of molecules that are chemically attached to the surface of nanoparticles plays a crucial role in target recognition. For example, Drew R. et al. experimented with different amounts of ligands during the modification of the MNP surface. The authors showed that the most optimal MNP for cell labeling were generated via the conjugation of 23 affibody $Z_{HER2:342}$ molecules to the surface of 30 nm MNP [31].

We assumed that along with binding efficiency, the different densities of targeted molecules on the surface of MNP can probably affect the pH-dependent behavior of MNP. To assess the binding efficacy of MNP to cancer cells at acidic pH values, we utilized various concentrations of affibody $Z_{HER2:342}$ molecules in the carbodiimide reaction. The number of affibody $Z_{HER2:342}$ molecules conjugated per particle was calculated based on NTA data and BCA protein assay and amounted from 24 to 238 affibody molecules per MNP for different conjugation conditions.

Affibody binding site includes arginine, tryptophan, and tyrosine, which are mainly involved in the formation of intermolecular hydrogen bonds with HER2 [32]. It can be assumed that in a more acidic pH range arginine undergoes protonation, while the electron density of polar molecules, namely, tyrosine and tryptophan molecules may be rearranged. Consequently, these changes may lead to a decrease in the binding affinity of the affibody to HER2. In particular, Fig. 4A displays that conjugates MNP-AF3 (114 molecules of affibody/MNP), MNP-AF4 (122 molecules of affibody/MNP), MNP-AF5 (238 molecules of affibody/MNP) demonstrated low binding efficiency to cancer cells in the slightly acidic pH range but exhibited the maximum binding capacity within the pH range of 7.0–8.0.

MNP-AF1 (24 molecules of affibody/MNP) and MNP-AF2 (57 molecules of affibody/MNP) conjugates showed effective cellular uptake in the pH range of 5.6–6.4 and reduced binding capacity in the pH range of 7.0–8.0 in contrast to MNP-AF3 – MNP-AF5 with the high number of affibody molecules on MNP. This trend may be related to the fact that since MNP were coated with carboxymethyl dextran, carboxyl groups were exposed on the surface of MPN. At lower pH levels, these carboxyl groups can undergo protonation, causing a shift in electron density. Due to the low number of affibody molecules on the nanoparticle surface, protonated carboxyl groups can lead to predominant electrostatic interactions and enhance the binding efficiency of MNP at slightly acidic pH.

3.7. The method for affibody-functionalized MNP decoration with non-active protein to achieve pH-dependent bell-shaped dependency of cellular uptake

The aforementioned data suggests that the local charge on the particle surface with various pH solutions plays a crucial role in the cellular uptake of nanoparticles along with specific interactions. To maintain constant the number of targeted affibody molecules on the surface of MNP and reduce the local charge of nanoparticles, we performed the chemical conjugation with the mixture of affibody and BSA. Firstly, the pH-dependence of BSA interaction with cancer cells in saline buffers was studied. BSA is a negatively charged protein within the pH range of 5.6–8.0 due to the isoelectric point of albumin of 4.5. Fig. S3 demonstrates that the maximal binding of MNP-BSA with the receptor HER2 was observed at pH value of 5.8, which is due to its proximity to the isoelectric point of BSA. In the next stage, the ability of albumin to hinder the binding specificity of affibody to the HER2 receptor was studied. As depicted in Fig. S2B, results of the flow cytometry method revealed that BSA did not significantly reduce the interaction efficiency of affibody with cancer cells. Thus, albumin was chosen for subsequent modification of the surface of nanoparticles without reducing their targeting effect.

During modification of the MNP surface with 2 types of proteins the affibody concentration was maintained constant (equal to that concentration that resulted in 114 affibody molecules per MNP), while several BSA concentrations were tested in combination with fixed affibody concentration.

The following conjugates of MNP were obtained: MNP-BSA (modified with BSA only), MNP-AF (modified with affibody only), MNP-AF-BSA1 (modified with BSA:affibody w/w ratio of 10:1), MNP-AF-BSA2 (modified with BSA:affibody w/w ratio of 3:1), and MNP-AF-BSA3 (modified with BSA:affibody w/w ratio of 1:1). Fig. 4B indicated that the efficiency of MNP binding to cells at different pH values varied depending on the amount of BSA used with the highest cellular uptake at BSA:affibody ratio of 1:1. Interestingly, each type of conjugate with affibody and BSA showed a bell-shaped dependency of interaction with HER2-positive cells within the pH range of 5.6–8.0, with the highest cellular uptake observed at pH 6.4 close to that of tumor microenvironment.

To elucidate the mechanism of such bell-shaped interaction, we measured the ζ-potential and hydrodynamic sizes of conjugates to determine any changes in MNP modified with BSA. However, the ζ-potentials of BSA-modified conjugates at standard pH value did not show any significant differences from the control conjugates (Fig. 4C). The same trend was observed for the hydrodynamic diameters of MNP, whereas the sizes were 286 ± 88 nm and 295 ± 73 nm for MNP-AF and MNP-AF-BSA, respectively (Fig. S4).

We proposed a possible mechanism for the formation of a bell-shaped dependence of MNP-AF-BSA interaction with cells, schematically illustrated in Fig. 4D. We assume that the main contribution is made by the charge characteristics of proteins on the surface of nanoparticles. In particular, BSA introduces local negative charges on the nanoparticle, while affibody remains a positively charged molecule. Thus, we reduce nonspecific interactions between nanoparticles and cells, while maintaining targeted delivery.

3.8. Biodistribution study of AFF MNP and AFF-BSA MNP in vivo and ex vivo

The efficacy of the developed method for chemical conjugation was proved by in vivo and ex vivo studies confirming the enhanced MNP delivery to HER2-positive tumors. Particularly, conjugates of MNP-AF and MNP-AF-BSA with BSA to affibody w/w ratio of 10:1 were utilized to compare the efficacy of MNP delivery and accumulation in the acidic tumor microenvironment in vivo.

To create the EMT-HER2 allograft tumor model, EMT-HER2 cancer cells were s.c. injected into BALB/c mice in the right flanks. The growth of the tumor was monitored for 14 days to establish an overgrown vasculature and reach the maximum level of acidification in the tumor microenvironment. Fluorescently labeled magnetic conjugates were i.v. injected into BALB/c mice with tumors. The accumulation of MNP was examined both in vivo and ex vivo 16 h after the injection of nanoparticles, and the accumulation dynamics of MNP in vivo are presented in Fig. S5.

A comparison between the accumulation efficiency of two types of magnetic conjugates was performed using the fluorescent tomograph LumoTrace Fluo (Abisense, Russia). Fluorescent images of mice after administration of MNP-AF and MNP-AF-BSA, along with the distribution of MNP in organs ex vivo, are presented in Fig. 5A. The distribution of the fluorescent signal in the extracted organs is shown in Fig. S6, however, the difference in the accumulation of the two types of MNP was not statistically significant.

Fluorescence detection is not a quantitative method for assessing the accumulation of nanoparticles in organs due to different light absorption and scattering by tissues, the presence of different autofluorescence signals in different organs, different depths of fluorescent labels, and a number of other factors. Therefore, we used the quantitative method for detection of magnetic materials to assess the biodistribution of MNP in mice. The MPQ technique (magnetic particle quantification) which is based on the detection of a magnetic signal with a high sensitivity limit and absence of a background signal from non-magnetic materials was used [28]. To get the distribution of MNP, magnetic signals of mouse organs were measured using the MPQ device for two groups of mice: mice injected with MNP-AF and mice injected with MNP-AF-BSA (n = 6 in each group). The efficiency of nanoparticle accumulation in tumors was 1.7 ± 0.7 % of the injected dose for the MNP-AF group and 3.4 ± 1.4 % for the MNP-AF-BSA group at the same administered dose of

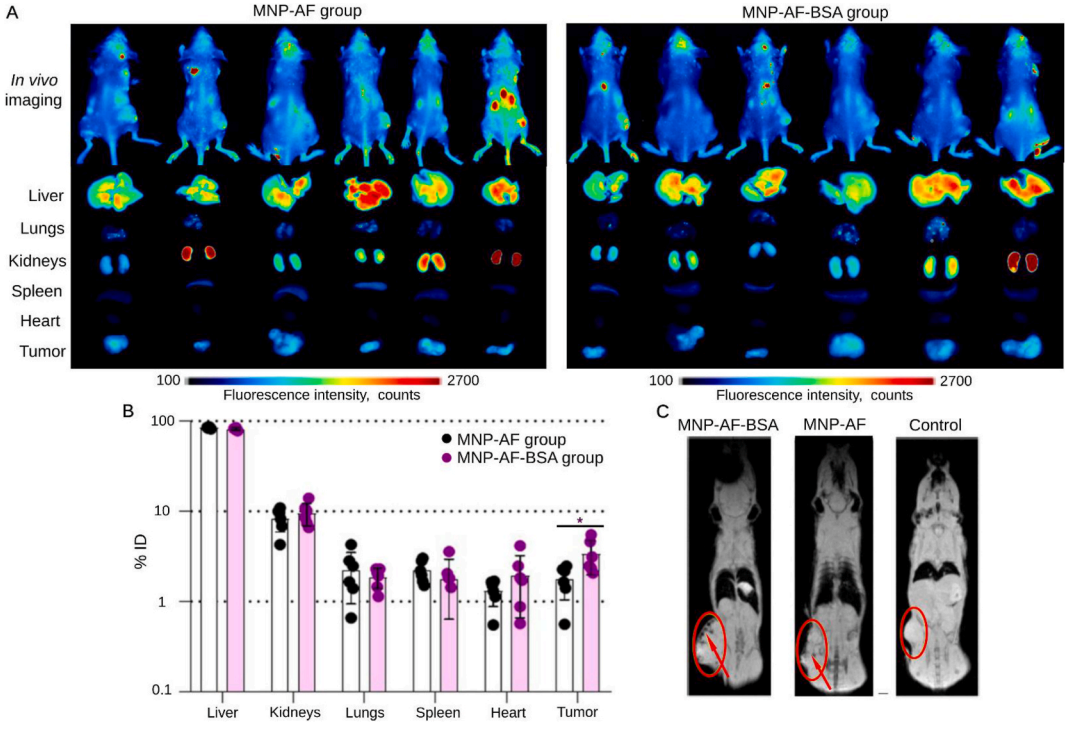

Fig. 5. Biodistribution of MNP-AF and MNP-AF-BSA in mice: in vivo imaging and ex vivo evaluation of MNP accumulation in tumors. (A) Fluorescent images of mice 16 h after i.v. injection of MNP and fluorescent images of extracted organs (λex = 630 nm, λem = 650 nm). (B) The percent of injected dose (ID) of MNP accumulated in organs that was measured with the MPQ technique. Data are presented in a logarithmic scale (n = 6 for each group). *p < 0.05. (C) Representative MRI images of nanoparticle distribution in tumors. The tumor boundaries are indicated by red circles. Higher MNP content corresponds to the darker color and is indicated by red arrows. (For interpretation of the references to color in this figure legend, the reader is referred to the Web version of this article.)

nanoparticles, which is presented in Fig. 5B. The statistical difference between groups was calculated using two-sided unequal variances t-tests and p-value was found to be 0.03, which indicates an effective improvement in the accumulation of MNP in tumor when using magnetic conjugates with affibody and BSA. The obtained results were visualized using MRI, images with accumulated MNP are shown in Fig. 5C.

As a result, incorporation of BSA into the HER2-specific MNP surface improves the efficiency of nanoparticles accumulation in the tumor, namely, the delivery of MNP-AF-BSA was 2 times higher than MNP-AF. Dual-modal nanoparticles MNP-AF-BSA provide enhanced tumor imaging capabilities through the utilization of three distinct physical analysis methods: detection of the fluorescence signal, non-linear magnetization (MPQ) and nuclear magnetic resonance (MRI).

4. Discussion

Nanomedicine has emerged as a highly promising field in cancer treatment, offering innovative approaches and solutions compared to conventional methods. With an enhanced understanding of tumorigenesis mechanisms, highly specific nanoagents that can bind to molecular cancer targets are being actively developed to generate new drug delivery strategies and minimize the side effects of the treatment.

The properties of nanoparticles, such as size, shape, surface chemistry, and charge, play a crucial role in their delivery efficacy to tumor targets in vivo. In particular, hydrophobic and strongly charged nanoparticles are recognized by immune cells and are quickly removed from the bloodstream before reaching tumor cells. To avoid this, nanoparticles are designed with a hydrophilic shell and neutral charge using polyethylene glycol (PEG). Currently, Caelyx is the PEGylated liposomal formulation of doxorubicin, which was approved in Europe and the United States for advanced ovarian cancer treatment [33]. However, PEGylation can also hide nanoparticles from cancer cells, reducing their targeted delivery efficiency. To address this, strategies have been developed to enhance nanoparticle delivery to cancer cells without modifying their surface or structure. One approach involves saturating macrophages with allogeneic anti-erythrocyte antibodies, which increases the circulation time of nanoparticles [34]. Another strategy is RBC-hitchhiking, where nanoparticles are delivered using red blood cells as a platform to avoid recognition and removal by macrophages [35]. The combination of targeted nanoparticles and the reduction of the immune response in vivo is the most effective platform for improving the delivery efficiency of nanoagents to tumor molecular targets, respectively.

During developing approaches for the therapy and diagnosis of tumors, nanoparticles can be effectively targeted to various biomarkers expressed on tumor cells, blood vessels, and immune cells. The receptor HER2 represents a crucial target due to the fact that HER2 oncomarker is overexpressed in 20–30 % of human breast carcinomas and other types of cancer [36,37], and high efficacy in the treatment of breast cancer is still not achieved [38]. Nanoagents can be specifically targeted to the HER2 receptor by utilizing various types of molecules, particularly, anti-HER2 antibodies [39–41], HER2-recognising affibodies [42–45], HER2-targeting proteins based on albumin-binding domains derived affinity proteins (ADAPTs) [46], HER2-specific DARPins (Designed Ankyrin Repeat Protein) [47], peptides with HER2 targeting moiety [48] and glycans [49].

The spectrum of cancer-specific nanoagents activities can be increased by designing nanoparticles that can effectively interact with tumor-associated targets in the pH range of the tumor microenvironment. Tumor cells maintain normal or alkaline intracellular pH and produce an increased amount of ions that are transported outside the cells, which leads to a shift in the extracellular pH value towards a more acidic region (pH 6.0–7.0) and acidification of the tumor microenvironment [50,51]. For effective delivery of nanoagents to the slightly acidic microenvironment of tumors, various approaches are being developed, including pH-sensitive peptides and pH-triggered ionized materials, triggered drug release and charge reversal of nanoagents [52–54]. Nevertheless, these materials possess certain drawbacks, in particular, the commonly employed pH-sensitive polymers are characterized by a lack of targeting and are unable to direct nanoparticles toward specific biomarkers. Additionally, when nanoparticles modified with pH-sensitive polymers interact with cells, they tend to exhibit a predominantly sigmoidal dependence on cellular uptake.

Our study was aimed to develop nanoparticles that effectively interact with cancer cells with a maximum cellular uptake in the pH values of the tumor microenvironment. To meet this challenge, we obtained monodisperse CMD-coated magnetic nanoparticles that are stable in saline solutions. Affibody $Z_{HER2:342}$ was selected for HER2-positive cancer cell targeting due to its successful application for imaging and elimination of cancer cells in many studies [57–59], which are presented in Supplemental Table S1. Affibody-functionalized MNP demonstrated high binding selectivity to cancer cells at a standard pH of 7.4, however, at slightly acidic pH, cellular uptake was reduced.

To alter the local charge on the MNP surface and improve cell*MNP interaction at tumor pH values, our approach involved the decoration of affibody-functionalized MNP with BSA during the chemical conjugation process. BSA has a pI value ranging from 4.5 to 4.8 [55], while the affibody is characterized by a pI value of 9.1. BSA is the main component of serum proteins of cows, which is derived from the blood serum. Due to BSA's high solubility, stability, and versatility in binding to a wide range of molecules, this protein is extensively utilized in numerous scientific applications, including cell culture, immunoassays, diagnostic tests, and molecular biology. Furthermore, BSA is well-suited for in vivo applications due to its non-immunogenic and non-toxic nature [56]. We obtained MNP-AF-BSA, which demonstrated a bell-shaped dependence of interaction with cancer cells in the pH values of tumor microenvironment with a maximal cellular uptake at pH value 6.4.

This mechanism is attributed to the following factors presented in Fig. 4D:

(i) At slightly acidic pH values, the binding of MNP-AF to cancer cells is hindered due to the affibody molecules. In the presence of a large number of hydrogen cations, affibody molecules are being protonated, including the protonation of amino acids of the recognition site of affibody binding to the HER2. As a result, the efficiency of affibody interaction with the receptor is

significantly lower at slightly acidic pH compared to more alkaline ones (Fig. 2D). This trend persists for both free affibody (Fig. 2D) and affibody on the surface of MNP-AF (Figs. 3 and 4A) and MNP-AF-BSA (Fig. 4B).

(ii) At alkaline pH values, the binding of MNP-BSA to cancer cells is impeded by BSA. BSA acquires a negative charge, similar to cancer cells, resulting in electrostatic repulsion and reduced cell binding. This tendency is observed for both MNP-BSA (Fig. S3) and MNP-AF-BSA (Fig. 4B).

(i) + (ii) = (iii) Therefore, the optimal binding range for MNP-AF-BSA to cancer cells is between pH 6.0 and 7.0, whereas affibody interaction with cancer cells increases linearly with pH, while that of BSA decreases, collectively superimposing in a bell-shaped dependence of nanoparticle*cell complexes formation.

The proposed mechanism of MNP-AF-BSA action was confirmed in vivo: incorporation of BSA into the HER2-specific MNP surface resulted in a two-fold increase in its accumulation in vivo in the tumor compared to MNP-AF. In the field of nanotechnology researcher's attention is mainly focused on the improving targeted nanoparticles accumulation in the tumor more than 1 % of administrated dose, whereas typical tumor accumulation rate accounts for 0.7 % [60]. We believe that the enhancement of the obtained MNP delivery in the tumor is noteworthy, taking into account that we achieved accumulation of MNP-AF delivery of 1.7 ± 0.7 % and improved this by using BSA to a rate of 3.4 ± 1.4 %.

Our findings regarding MNPs biodistribution, including significant accumulation in the liver, are consistent with previously reported studies on similar particles [61–63]. Magnetic nanoparticles are known for its biodegradability and low systemic toxicity as evidenced in the corresponding study [61]. Therefore, no significant toxicity is anticipated from the accumulation of MNPs in various organs of mice with further use of nanoparticles for various biomedical applications.

We successfully enhanced the specificity of HER2-targeted MNP delivery to cancer cells by the addition of non-active BSA protein on the surface of MNP without using pH-sensitive materials. However, this modification can only be used for nanoagents that possess carboxyl groups on their surface. In our study, we selected the optimal ratio of affibody and non-active protein, for another HER2-targeting molecule it would be essential to re-evaluate the appropriate ratio with the stabilizing protein, considering the distinct sizes and structural properties of HER2-specific molecules. Here we created magnetic nanoparticles modified with HER2-specific molecules and non-active BSA for successful delivery to HER2-positive tumors at slightly acidic pH levels. A combination of targeting nanoparticles to receptor HER2 and the pH of the tumor microenvironment could be applied to other nanomaterials to improve the accumulation of nanoagents in the tumor. The obtained magnetic conjugates represent promising agents for oncotheranostics due to their ability for tumor targeting and bioimaging, magnetic hyperthermia induction, and mechanical destruction of cancer cells under the influence of external magnetic fields.

5. Conclusion

Our research demonstrated the successful method of enhancing targeted MNP delivery to cancer cells without changing functional molecules of nanomaterial. In this work, we showed that the combination of targeting and stabilizing proteins on the surface of nanoparticles forms a bell-shaped dependency of MNP cellular uptake and improves nanoagents accumulation in tumor. Based on these findings, we strongly believe that targeting nanoparticles to the acidic pH of the tumor microenvironment will significantly improve the delivery efficiency of existing nanocarriers and result in notable advancements in tumor therapy and diagnostics.

Ethics statement

All experimental procedures with animals were approved by the Institutional Animal Care and Use Committee (IACUC) of the Shemyakin-Ovchinnikov Institute of Bioorganic Chemistry Russian Academy of Sciences, protocol # 375/2023 (September 20, 2023–September 19, 2026).

CRediT authorship contribution statement

Olga A. Kolesnikova: Investigation, Methodology, Visualization, Writing – original draft. **Elena N. Komedchikova:** Investigation, Methodology. **Svetlana D. Zvereva:** Methodology. **Anastasiia S. Obozina:** Methodology, Visualization. **Olha V. Dorozh:** Methodology. **Iurii Afanasev:** Methodology. **Petr I. Nikitin:** Methodology. **Elizaveta N. Mochalova:** Investigation, Methodology. **Maxim P. Nikitin:** Funding acquisition, Investigation, Resources, Validation. **Victoria O. Shipunova:** Conceptualization, Formal analysis, Funding acquisition, Investigation, Methodology, Project administration, Resources, Supervision, Validation, Visualization, Writing – original draft.

Declaration of competing interest

The authors declare that they have no known competing financial interests or personal relationships that could have appeared to influence the work reported in this paper.

Acknowledgments

Different parts of this study were supported by MSHE of RF, agreement 075-03-2024-117, project FSMG-2023-0015 (decoration of

the nanoparticle surface with affibody and BSA, and quantification of the number of molecules on nanoparticle surface, affibody purification and characterization), FSMG-2023-0017 (analysis of targeted nanoparticle binding with cells by flow cytometry), FSMG-2022-0016 (in vivo biodistribution study), and Russian Science Foundation project N№ 24-13-20032 (magnetic nanoparticle synthesis and characterization).

Appendix A. Supplementary data

Supplementary data to this article can be found online at https://doi.org/10.1016/j.heliyon.2024.e34211.

References

[1] C. Xia, X. Dong, H. Li, M. Cao, D. Sun, S. He, F. Yang, X. Yan, S. Zhang, N. Li, W. Chen, Cancer statistics in China and United States, 2022: profiles, trends, and determinants, Chinese Med J 135 (5) (2022) 584–590, https://doi.org/10.1097/CM9.0000000000002108.
[2] R.L. Siegel, K.D. Miller, N.S. Wagle, A. Jemal, Cancer statistics, 2023, CA A Cancer J. Clin. 73 (1) (2023) 17–48, https://doi.org/10.3322/caac.21763.
[3] H. Sung, J. Ferlay, R.L. Siegel, M. Laversanne, I. Soerjomataram, A. Jemal, F. Bray, Global cancer statistics 2020: GLOBOCAN estimates of incidence and mortality worldwide for 36 cancers in 185 countries, CA A Cancer J. Clin. 71 (3) (2021) 209–249, https://doi.org/10.3322/caac.21660.
[4] V.S. Madamsetty, A. Mukherjee, S. Mukherjee, Recent trends of the bio-inspired nanoparticles in cancer theranostics, Front. Pharmacol. 10 (2019) 1264, https://doi.org/10.3389/fphar.2019.01264.
[5] S. Zhao, X. Yu, Y. Qian, W. Chen, J. Shen, Multifunctional magnetic iron oxide nanoparticles: an advanced platform for cancer theranostics, Theranostics 10 (14) (2020) 6278–6309, https://doi.org/10.7150/thno.42564.
[6] X. Li, W. Li, M. Wang, Z. Liao, Magnetic nanoparticles for cancer theranostics: advances and prospects, J. Contr. Release 335 (2021) 437–448, https://doi.org/10.1016/j.jconrel.2021.05.042.
[7] C. Nieto, M.A. Vega, Martín del Valle, E.M. Trastuzumab, More than a guide in HER2-positive cancer nanomedicine, Nanomaterials 10 (9) (2020) 1674, https://doi.org/10.3390/nano10091674.
[8] V.O. Shipunova, O.A. Kolesnikova, P.A. Kotelnikova, V.D. Soloviev, A.A. Popov, G.M. Proshkina, M.P. Nikitin, S.M. Deyev, Comparative evaluation of engineered polypeptide scaffolds in HER2-targeting magnetic nanocarrier delivery, ACS Omega 6 (24) (2021) 16000–16008, https://doi.org/10.1021/acsomega.1c01811.
[9] V.O. Shipunova, S.M. Deyev, Artificial scaffold PolypeptidesAs an efficient tool for the targeted delivery of nanostructures in vitro and in vivo, Acta Naturae 14 (1) (2022) 54–72, https://doi.org/10.32607/actanaturae.11545.
[10] J. Löfblom, J. Feldwisch, V. Tolmachev, J. Carlsson, S. Ståhl, F.Y. Frejd, Affibody molecules: engineered proteins for therapeutic, diagnostic and biotechnological applications, FEBS (Fed. Eur. Biochem. Soc.) Lett. 584 (12) (2010) 2670–2680, https://doi.org/10.1016/j.febslet.2010.04.014.
[11] S. Ståhl, T. Gräslund, A. Eriksson Karlström, F.Y. Frejd, P.-Å. Nygren, J. Löfblom, Affibody molecules in biotechnological and medical applications, Trends Biotechnol. 35 (8) (2017) 691–712, https://doi.org/10.1016/j.tibtech.2017.04.007.
[12] F.Y. Frejd, K.-T. Kim, Affibody molecules as engineered protein drugs, Exp. Mol. Med. 49 (3) (2017) e306, https://doi.org/10.1038/emm.2017.35, e306.
[13] R. Luo, H. Liu, Z. Cheng, Protein scaffolds: antibody alternatives for cancer diagnosis and therapy, RSC Chem. Biol. 3 (7) (2022) 830–847, https://doi.org/10.1039/D2CB00094F.
[14] X. Hu, D. Li, Y. Fu, J. Zheng, Z. Feng, J. Cai, P. Wang, Advances in the application of radionuclide-labeled HER2 affibody for the diagnosis and treatment of ovarian cancer, Front. Oncol. 12 (2022) 917439, https://doi.org/10.3389/fonc.2022.917439.
[15] Yu A. Koksharov, S.P. Gubin, I.V. Taranov, G.B. Khomutov, Yu V. Gulyaev, Magnetic nanoparticles in medicine: progress, problems, and advances, J. Commun. Technol. Electron. 67 (2) (2022) 101–116, https://doi.org/10.1134/S1064226922020073.
[16] E. Boedtkjer, S.F. Pedersen, The acidic tumor microenvironment as a driver of cancer, Annu. Rev. Physiol. 82 (1) (2020) 103–126, https://doi.org/10.1146/annurev-physiol-021119-034627.
[17] K. Na, E. Seong Lee, Y.H. Bae, Adriamycin loaded pullulan acetate/sulfonamide conjugate nanoparticles responding to tumor PH: PH-dependent cell interaction, internalization and cytotoxicity in vitro, J. Contr. Release 87 (1–3) (2003) 3–13, https://doi.org/10.1016/S0168-3659(02)00345-0.
[18] E.S. Lee, K.T. Oh, D. Kim, Y.S. Youn, Y.H. Bae, Tumor PH-responsive flower-like micelles of poly(l-lactic acid)-b-poly(ethylene glycol)-b-poly(l-histidine), J. Contr. Release 123 (1) (2007) 19–26, https://doi.org/10.1016/j.jconrel.2007.08.006.
[19] F.P. Seib, G.T. Jones, J. Rnjak-Kovacina, Y. Lin, D.L. Kaplan, PH-dependent anticancer drug release from silk nanoparticles, Adv. Healthcare Mater. 2 (12) (2013) 1606–1611, https://doi.org/10.1002/adhm.201300034.
[20] A. Madhusudhan, G. Reddy, M. Venkatesham, G. Veerabhadram, D. Kumar, S. Natarajan, M.-Y. Yang, A. Hu, S. Singh, Efficient PH dependent drug delivery to target cancer cells by gold nanoparticles capped with carboxymethyl chitosan, IJMS 15 (5) (2014) 8216–8234, https://doi.org/10.3390/ijms15058216.
[21] S. Sengottiyan, A. Mikolajczyk, T. Puzyn, How does the study MD of pH-dependent exposure of nanoparticles affect cellular uptake of anticancer drugs? Int. J. Mol. Sci. 24 (4) (2023) 3479, https://doi.org/10.3390/ijms24043479.
[22] V.O. Shipunova, E.N. Komedchikova, P.A. Kotelnikova, M.P. Nikitin, S.M. Deyev, Targeted two-step delivery of oncotheranostic nano-PLGA for HER2-positive tumor imaging and therapy in vivo: improved effectiveness compared to one-step strategy, Pharmaceutics 15 (3) (2023) 833, https://doi.org/10.3390/pharmaceutics15030833.
[23] V.O. Shipunova, M.P. Nikitin, P.I. Nikitin, S.M. Deyev, MPQ-cytometry: a magnetism-based method for quantification of nanoparticle–cell interactions, Nanoscale 8 (25) (2016) 12764–12772, https://doi.org/10.1039/C6NR03507H.
[24] E.N. Mochalova, E.A. Egorova, K.S. Komarova, V.O. Shipunova, N.F. Khabibullina, P.I. Nikitin, M.P. Nikitin, Comparative study of nanoparticle blood circulation after forced clearance of own erythrocytes (mononuclear phagocyte system-cytoblockade) or administration of cytotoxic doxorubicin- or clodronate-loaded liposomes, IJMS 24 (13) (2023) 10623, https://doi.org/10.3390/ijms241310623.
[25] M.P. Nikitin, V.O. Shipunova, S.M. Deyev, P.I. Nikitin, Biocomputing based on particle disassembly, Nat. Nanotechnol. 9 (9) (2014) 716–722, https://doi.org/10.1038/nnano.2014.156.
[26] V.O. Shipunova, E.N. Komedchikova, P.A. Kotelnikova, I.V. Zelepukin, A.A. Schulga, G.M. Proshkina, E.I. Shramova, H.L. Kutscher, G.B. Telegin, A.V. Kabashin, P.N. Prasad, S.M. Deyev, Dual regioselective targeting the same receptor in nanoparticle-mediated combination immuno/chemotherapy for enhanced image-guided cancer treatment, ACS Nano 14 (10) (2020) 12781–12795, https://doi.org/10.1021/acsnano.0c03421.
[27] K. Yamatsugu, H. Katoh, T. Yamashita, K. Takahashi, S. Aki, T. Tatsumi, Y. Kaneko, T. Kawamura, M. Miura, M. Ishii, K. Ohkubo, T. Osawa, T. Kodama, S. Ishikawa, M. Kanai, A. Sugiyama, Antibody mimetic drug conjugate manufactured by high-yield Escherichia coli expression and non-covalent binding system, Protein Expr. Purif. 192 (2022) 106043, https://doi.org/10.1016/j.pep.2021.106043.
[28] A. Orlova, M. Magnusson, T.L.J. Eriksson, M. Nilsson, B. Larsson, I. Höidén-Guthenberg, C. Widström, J. Carlsson, V. Tolmachev, S. Ståhl, F.Y. Nilsson, Tumor imaging using a picomolar affinity HER2 binding affibody molecule, Cancer Res. 66 (8) (2006) 4339–4348, https://doi.org/10.1158/0008-5472.CAN-05-3521.
[29] F. Fleetwood, S. Klint, M. Hanze, E. Gunneriusson, F.Y. Frejd, S. Ståhl, J. Löfblom, Simultaneous targeting of two ligand-binding sites on VEGFR2 using biparatopic affibody molecules results in dramatically improved affinity, Sci. Rep. 4 (1) (2014) 7518, https://doi.org/10.1038/srep07518.

[30] A.-C. Steffen, Y. Almqvist, M.-K. Chyan, H. Lundqvist, V. Tolmachev, D. Wilbur, J. Carlsson, Biodistribution of 211At labeled HER-2 binding affibody molecules in mice, Oncol. Rep. (2007), https://doi.org/10.3892/or.17.5.1141.

[31] R. Elias Drew, A. Poloukhtine, V. Popik, A. Tsourkas, Effect of ligand density, receptor density, and nanoparticle size on cell targeting, Nanomed. Nanotechnol. Biol. Med. 9 (2) (2013) 194–201, https://doi.org/10.1016/j.nano.2012.05.015.

[32] C. Eigenbrot, M. Ultsch, A. Dubnovitsky, L. Abrahmsén, T. Härd, Structural basis for high-affinity HER2 receptor binding by an engineered protein, Proc. Natl. Acad. Sci. U.S.A. 107 (34) (2010) 15039–15044, https://doi.org/10.1073/pnas.1005025107.

[33] P.S. S, R.V. Nagarkar, K.C. Puligundla, L.K. N, R.R. Boya, A.B. Patel, L. Goyal, A. Thoke, J.G. Patel, A.O. Mehta, G.N. Patel, M.A. Khan, I. Ahmad, Bioequivalence of a hybrid pegylated liposomal doxorubicin hydrochloride injection and Caelyx®: a single-dose, randomized, multicenter, open-label, two-period crossover study in patients with advanced ovarian cancer, Eur. J. Pharmaceut. Sci. 176 (2022) 106248, https://doi.org/10.1016/j.ejps.2022.106248.

[34] M.P. Nikitin, I.V. Zelepukin, V.O. Shipunova, I.L. Sokolov, S.M. Deyev, P.I. Nikitin, Enhancement of the blood-circulation time and performance of nanomedicines via the forced clearance of erythrocytes, Nat. Biomed. Eng. 4 (7) (2020) 717–731, https://doi.org/10.1038/s41551-020-0581-2.

[35] I.V. Zelepukin, A.V. Yaremenko, V.O. Shipunova, A.V. Babenyshev, I.V. Balalaeva, P.I. Nikitin, S.M. Deyev, M.P. Nikitin, Nanoparticle-based drug delivery *via* RBC-hitchhiking for the inhibition of lung metastases growth, Nanoscale 11 (4) (2019) 1636–1646, https://doi.org/10.1039/C8NR07730D.

[36] A. Patel, N. Unni, Y. Peng, The changing paradigm for the treatment of HER2-positive breast cancer, Cancers 12 (8) (2020) 2081, https://doi.org/10.3390/cancers12082081.

[37] S. Loibl, L. Gianni, HER2-Positive breast cancer, Lancet 389 (10087) (2017) 2415–2429, https://doi.org/10.1016/S0140-6736(16)32417-5.

[38] I. Schlam, S.M. Swain, HER2-Positive breast cancer and tyrosine kinase inhibitors: the time is now, npj Breast Cancer 7 (1) (2021) 56, https://doi.org/10.1038/s41523-021-00265-1.

[39] J.S. Chen, J. Chen, S. Bhattacharjee, Z. Cao, H. Wang, S.D. Swanson, H. Zong, J.R. Baker, S.H. Wang, Functionalized nanoparticles with targeted antibody to enhance imaging of breast cancer in vivo, J. Nanobiotechnol. 18 (1) (2020) 135, https://doi.org/10.1186/s12951-020-00695-2.

[40] M.R. Abedin, K. Powers, R. Aiardo, D. Barua, S. Barua, Antibody–drug nanoparticle induces synergistic treatment efficacies in HER2 positive breast cancer cells, Sci. Rep. 11 (1) (2021) 7347, https://doi.org/10.1038/s41598-021-86762-6.

[41] A.H. Haghighi, Z. Faghih, M.T. Khorasani, F. Farjadian, Antibody conjugated onto surface modified magnetic nanoparticles for separation of HER2+ breast cancer cells, J. Magn. Magn Mater. 490 (2019) 165479, https://doi.org/10.1016/j.jmmm.2019.165479.

[42] H. Wang, D. Jia, D. Yuan, X. Yin, F. Yuan, F. Wang, W. Shi, H. Li, L.-M. Zhu, Q. Fan, Dimeric her2-specific affibody mediated cisplatin-loaded nanoparticles for tumor enhanced chemo-radiotherapy, J. Nanobiotechnol. 19 (1) (2021) 138, https://doi.org/10.1186/s12951-021-00885-6.

[43] M. Moballegh-Nasery, A. Mandegary, T. Eslaminejad, M. Zeinali, A. Pardakhti, B. Behnam, M. Mohammadi, Cytotoxicity evaluation of curcumin-loaded affibody-decorated liposomes against breast cancerous cell lines, J. Liposome Res. 31 (2) (2021) 189–194, https://doi.org/10.1080/08982104.2020.1755981.

[44] V.O. Shipunova, A.S. Sogomonyan, I.V. Zelepukin, M.P. Nikitin, S.M. Deyev, PLGA nanoparticles decorated with anti-HER2 affibody for targeted delivery and photoinduced cell death, Molecules 26 (13) (2021) 3955, https://doi.org/10.3390/molecules26133955.

[45] V.O. Shipunova, M.M. Belova, P.A. Kotelnikova, O.N. Shilova, A.B. Mirkasymov, N.V. Danilova, E.N. Komedchikova, R. Popovtzer, S.M. Deyev, M.P. Nikitin, Photothermal therapy with HER2-targeted silver nanoparticles leading to cancer remission, Pharmaceutics 14 (5) (2022) 1013, https://doi.org/10.3390/pharmaceutics14051013.

[46] R. Mahmoudi, H. Dianat-Moghadam, M. Poorebrahim, S. Siapoush, V. Poortahmasebi, R. Salahlou, M. Rahmati, Recombinant immunotoxins development for HER2-based targeted cancer therapies, Cancer Cell Int. 21 (1) (2021) 470, https://doi.org/10.1186/s12935-021-02182-6.

[47] P. Wild, R. Eapen, P. Forrer, C. Jost, *The DARPin Encyclopedia: from Basic Research Towards Therapeutics*; Preprint, LIFE SCIENCES, 2022, https://doi.org/10.20944/preprints202206.0147.v3.

[48] B. Kim, J. Shin, J. Wu, D.T. Omstead, T. Kiziltepe, L.E. Littlepage, B. Bilgicer, Engineering peptide-targeted liposomal nanoparticles optimized for improved selectivity for HER2-positive breast cancer cells to achieve enhanced in vivo efficacy, J. Contr. Release 322 (2020) 530–541, https://doi.org/10.1016/j.jconrel.2020.04.010.

[49] Y. Dong, W. Li, Z. Gu, R. Xing, Y. Ma, Q. Zhang, Z. Liu, Inhibition of HER2-positive breast cancer growth by blocking the HER2 signaling pathway with HER2-glycan-imprinted nanoparticles, Angew. Chem. Int. Ed. 58 (31) (2019) 10621–10625, https://doi.org/10.1002/anie.201904860.

[50] E.S. Lee, Z. Gao, Y.H. Bae, Recent progress in tumor PH targeting nanotechnology, J. Contr. Release 132 (3) (2008) 164–170, https://doi.org/10.1016/j.jconrel.2008.05.003.

[51] X. Zhang, Y. Lin, R.J. Gillies, Tumor PH and its measurement, J. Nucl. Med. 51 (8) (2010) 1167–1170, https://doi.org/10.2967/jnumed.109.068981.

[52] N.U. Dharmaratne, A.R. Kaplan, P.M. Glazer, Targeting the hypoxic and acidic tumor microenvironment with PH-sensitive peptides, Cells 10 (3) (2021) 541, https://doi.org/10.3390/cells10030541.

[53] N.M. AlSawaftah, N.S. Awad, W.G. Pitt, G.A. Husseini, PH-responsive nanocarriers in cancer therapy, Polymers 14 (5) (2022) 936, https://doi.org/10.3390/polym14050936.

[54] B. Chen, W. Dai, B. He, H. Zhang, X. Wang, Y. Wang, Q. Zhang, Current multistage drug delivery systems based on the tumor microenvironment, Theranostics 7 (3) (2017) 538–558, https://doi.org/10.7150/thno.16684.

[55] W. Ang, M. Elimelech, Protein (BSA) fouling of reverse osmosis membranes: implications for wastewater reclamation, J. Membr. Sci. 296 (1–2) (2007) 83–92, https://doi.org/10.1016/j.memsci.2007.03.018.

[56] J. Wang, B. Zhang, Bovine serum albumin as a versatile platform for cancer imaging and therapy, Comput. Mater. Continua (CMC) 25 (25) (2018) 2938–2953, https://doi.org/10.2174/0929867324666170314143335.

[57] M. Moballegh-Nasery, A. Mandegary, T. Eslaminejad, M. Zeinali, A. Pardakhti, B. Behnam, M. Mohammadi, Cytotoxicity evaluation of curcumin-loaded affibody-decorated liposomes against breast cancerous cell lines, J. Liposome Res. 31 (2) (2021) 189–194, https://doi.org/10.1080/08982104.2020.1755981.

[58] M. Ghanemi, A. Pourshohod, M.A. Ghaffari, A. kheirollah, M. Amin, M. Zeinali, M. Jamalan, Specific targeting of HER2-positive head and neck squamous cell carcinoma line HN5 by idarubicin-ZHER2 affibody conjugate, CCDT 19 (1) (2018) 65–73, https://doi.org/10.2174/1568009617666170427105417.

[59] V. Tolmachev, T.J. Grönroos, C.-B. Yim, J. Garousi, Y. Yue, S. Grimm, J. Rajander, A. Perols, M. Haaparanta-Solin, O. Solin, R. Ferdani, A. Orlova, C.J. Anderson, A.E. Karlström, Molecular design of radiocopper-labelled affibody molecules, Sci. Rep. 8 (1) (2018) 6542, https://doi.org/10.1038/s41598-018-24785-2.

[60] S. Wilhelm, A. Tavares, Q. Dai, S. Ohta, J. Audet, H.F. Dvorak, W.C.W. Chan, Analysis of nanoparticle delivery to tumours, Nat. Rev. Mater. 1 (2016) 16014, https://doi.org/10.1038/natrevmats.2016.

[61] I.V. Zelepukin, A.V. Yaremenko, I.N. Ivanov, M.V. Yuryev, V.R. Cherkasov, S.M. Deyev, P.I. Nikitin, M.P. Nikitin, Long-term fate of magnetic particles in mice: a comprehensive study, ACS Nano 15 (7) (2021) 11341–11357, https://doi.org/10.1021/acsnano.1c00687.

[62] L.Y. Jie, L.L. Cai, L.J. Wang, X.Y. Ying, R.S. Yu, M.M. Zhang, Y.Z. Du, Actively-targeted LTVSPWY peptide-modified magnetic nanoparticles for tumor imaging, Int. J. Nanomed. 7 (2012) 3981–3989. https://doi:10.2147/IJN.S33593.

[63] J. Xie, K. Chen, J. Huang, S. Lee, J. Wang, J. Gao, X. Li, X. Chen, PET/NIRF/MRI triple functional iron oxide nanoparticles, Biomaterials 31 (11) (2010) 3016–3022. https://doi:10.1016/j.biomaterials.2010.01.010.